CHIN. PHYS. LETT. Vol. 38, No. 6 (2021) 064201

Broadband Sheet Parametric Oscillator for $\chi^{(2)}$ Optical Frequency Comb Generation via Cavity Phase Matching

Xin Ni(倪鑫)[1], Kunpeng Jia(贾琨鹏)[1], Xiaohan Wang(汪小涵)[1], Huaying Liu(刘华颖)[1], Jian Guo(郭健)[1], Shu-Wei Huang(黄书伟)[2], Baicheng Yao(姚佰承)[3], Nicolò Sernicola[1,4], Zhenlin Wang(王振林)[1], Xinjie Lv(吕新杰)[1*], Gang Zhao(赵刚)[1*], Zhenda Xie(谢臻达)[1*], and Shi-Ning Zhu(祝世宁)[1]

[1]*National Laboratory of Solid State Microstructures, School of Electronic Science and Engineering, School of Physics, and College of Engineering and Applied Sciences, Nanjing University, Nanjing 210093, China*
[2]*Department of Electrical, Computer, and Energy Engineering, University of Colorado Boulder, Boulder, CO 80301, USA*
[3]*Key Laboratory of Optical Fiber Sensing and Communications (Ministry of Education), University of Electronic Science and Technology of China, Chengdu 611731, China*
[4]*Institute for Optics, Information and Photonics, Friedrich-Alexander-Universität Erlangen-Nürnberg, Schloßplatz 4, Erlangen 91054, Germany*

(Received 3 February 2021; accepted 24 March 2021; published online 25 May 2021)

We demonstrate a broadband optical parametric oscillation, using a sheet cavity, via cavity phase-matching. A 21.2 THz broad comb-like spectrum is achieved, with a uniform line spacing of 133.0 GHz, despite a relatively large dispersion of 275.4 fs^2/mm around 1064 nm. With 22.6% high slope efficiency, and 14.9 kW peak power handling, this sheet optical parametric oscillator can be further developed for $\chi^{(2)}$ comb.

DOI: 10.1088/0256-307X/38/6/064201

Coherent radiation with pristine frequency spacings, or an optical frequency comb, is a measure of optical frequency, facilitating a revolutionary precision metrology, with potential for use in a variety of applications.[1−11] Such applications would benefit from miniaturized comb sources for portable devices with high beat-note frequencies, which are not available with conventional mode-locked laser sources, but whose requirements may potentially be met by virtue of the recent development of micro-optical parametric oscillators (μOPOs). To date, research has tended to focus on the micro-ring μOPOs with third-order nonlinearity, $\chi^{(3)}$.[12−18] A high-quality factor Q is key to the enhancement of the relatively weak third-order parametric processes in these micro-ring μOPOs, in order to lower the parametric threshold. However, such high Q also enforces strict phase-matching conditions, because the effective nonlinear interaction length increases as the Q value scales up. Therefore, the dispersion needs to be perfectly engineered over a large comb span, which is normally a challenge for μOPOs, and must limit the central wavelength for a given material. On the other hand, parametric oscillation can also be generated using second-order nonlinearity, $\chi^{(2)}$,[19−27] which is much stronger than $\chi^{(3)}$, and represents a novel approach to μOPO combs. Our experimental and other earlier theoretical works have shown that cavity phase matching (CPM)[28−34] can be realized in doubly-resonant $\chi^{(2)}$ Fabry–Pérot micro-cavities,[35] where the strict material phase-matching is not necessary, as the phase mismatch is corrected by the total reflection on the cavity mirrors for each round trip. Although the effective nonlinear interaction length can still be greatly extended while Q increases, the CPM condition is only dependent on cavity length, and results in a large bandwidth.

In this work, such a large CPM bandwidth plays a crucial role in achieving broadband parametric oscillation with a comb-like spectrum. Two types of sheet optical parametric oscillators (SOPOs) are fabricated, with different cavity lengths. Broad bandwidth can be achieved from these SOPOs by means of a $\chi^{(2)}$ CPM optical parametric down-conversion process, which exceeds 21.2 THz and 14.3 THz, with spectral line spacings of about 133.0 GHz and 514.0 GHz, respectively. By virtue of a strong second-order nonlinearity, such sub-millimeter SOPOs are capable of 22.6% slope efficiency, and 14.9 kW peak power. Despite a normal dispersion of 275.4 fs^2/mm, the line spacings are measured to be equidistant within the accuracy of a high-performance wavelength meter, which is less than the transform-limited linewidth. These results reveal the line-to-line nonlinear interactions that automatically lock the line spacings, and are verified by our simulation results. This simulation also exhibits lower noise

Supported by the National Key Research and Development Program of China (Grant Nos. 2019YFA0705000 and 2017YFA0303700), the Key R&D Program of Guangdong Province (Grant No. 2018B030329001), the Leading-Edge Technology Program of Jiangsu Natural Science Foundation (Grant No. BK20192001), and the National Natural Science Foundation of China (Grant Nos. 51890861, 11690031, 11621091, and 11674169).
*Corresponding authors. Email: xiezhenda@nju.edu.cn; zhaogang@nju.edu.cn; lvxinjie@nju.edu.cn
© 2021 Chinese Physical Society and IOP Publishing Ltd

under a cw pump, which may be used for optical frequency comb generation.

As first proposed by Armstrong *et al.* in 1962,[28] and our earlier experimental demonstration,[34] a sub-coherence-length Fabry–Pérot nonlinear cavity can generate a second-order nonlinear process by cavity phase-matching. The π phase shift gained from the reflection on the cavity mirrors compensates for the phase-mismatch of the light waves when they recirculate inside the cavity,[32,34] as the pump light is always in phase with the signal and idler when they recirculate inside the sheet cavity. Efficient frequency conversion can be achieved if the following first-order CPM condition is satisfied:

$$l_{\mathrm{cav}} \leqslant l_{\mathrm{coh}} = \frac{\pi}{k_{\mathrm{p}} - k_{\mathrm{s}} - k_{\mathrm{i}}}, \tag{1}$$

where l_{cav} is the cavity length, l_{coh} is the coherence length of the three-wave coupling, k_{p}, k_{s} and k_{i} are the wave vectors of pump, signal, and idler, respectively. We introduce the effective nonlinear coefficient, d_{eff}, to describe the strength of the nonlinear coupling, in place of the nonlinear coefficient, d_{31}, of the material, which is given by

$$d_{\mathrm{eff}} = d_{31}\left|\mathrm{sinc}\left(\frac{\pi l_{\mathrm{cav}}}{2l_{\mathrm{coh}}}\right)\right|. \tag{2}$$

In a doubly resonant SOPO, both CPM and longitudinal mode-matching conditions need to be satisfied with respect to the resonance modes. Despite the large CPM bandwidth, the longitudinal mode-matching results in strong frequency mode selectivity in the parametric beams. As shown in our previous work, tunable single-longitudinal-mode parametric oscillation can be achieved for SOPO via nondegenerate signal and idler modes, either in polarization or in frequency. In this study, however, degenerate type-I CPM SOPO is selected, so that more than one pair of modes can be excited at the same time. As shown in Fig. 1(a), two types of SOPOs are fabricated from fine-polished monolithic crystal y-cut MgO-doped lithium niobate crystal, at thicknesses of 140 μm and 485.25 μm, respectively. The type-I CPM process is phase-matched in the y-cut SOPOs so that larger coherence length can be achieved. The surface areas are both 5 mm × 5 mm in the xz plane. The two end faces of these crystal sheets are both anti-reflection coated for 532 nm (reflectivity $R < 1\%$), and high-reflection coated in the 900–1150 nm range, with $R > 99.8\%$ for the input surface, and $R = 97.0\%$ for the output surface. The Q values measure 6.6×10^4 and 1.9×10^5 for the 140 μm and 485.25 μm SOPOs, respectively. The type-I CPM process is designed to be phase-matched between the z-polarized pump at 532 nm, with x-polarized parametric beams centered around 1064 nm. Based on the temperature-dependent Sellmeier equation,[36,37] simulations show that the above parametric down-conversion process can be naturally phase-matched at 114°C, and CPM can be used to extend the phase-matching bandwidth, a prerequisite for comb generation. Figure 1(b) shows the calculated coherence length in comparison to the cavity lengths (denoted by red and blue lines) over a wavelength range from 900 nm to 1300 nm. It also includes the d_{eff} calculation for both SOPOs, based on Eq. (2). According to Eq. (1), CPM bandwidths of 351 nm and 183.1 nm can be expected for the above two SOPOs, respectively.

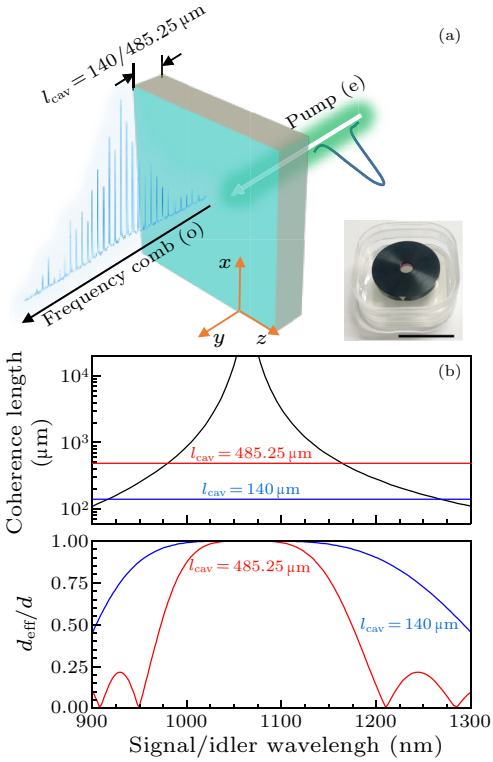

Fig. 1. The schematic of the broadband SOPO generation. (a) Design of SOPOs. Two types of SOPOs are fabricated, with cavity lengths of 140 μm and 485.25 μm, respectively. Inset: an image of our SOPO sample, with aluminum mount. (b) Coherence length and d_{eff} calculation. In the upper figure, the solid blue and red lines mark the CPM condition, where $l_{\mathrm{cav}} = l_{\mathrm{coh}}$ for different cavity lengths. In the lower figure, blue and red lines indicate d_{eff} as a function of signal/idler wavelengths for $l_{\mathrm{cav}} = 140$ μm and 485.25 μm.

In our experiment, the SOPOs are pumped by a single-longitudinal-mode frequency-doubled yttrium-aluminum-garnet laser (Powerlite, Continuum, Santa Clara, CA), with a pulse duration of 10 ns, and a repetition rate of 10 Hz. The average power drift of the YAG laser over eight hours, where $\Delta T = \pm 3$ ℃, is 5%. A solid pinhole is put inside the laser cavity to purify the transverse mode. The output is focused onto another pinhole to enable further selection of the TEM_{00} mode, and is imaged onto the SOPO with a beam full width at half maximum of 500 μm. The SOPO is embedded in a temperature-controllable oven with an accuracy better than 10 mK. The natural phase-matching temperature for our SOPO measures 111 ℃,

which is in good agreement with the theoretical value. We scan the temperature around 111 ℃; parametric oscillation output can be observed once the pump frequency is matched with the cavity modes for the signal and idler. A single-shot spectrum of the output is captured by a CCD-camera spectrometer (Acton 500, Princeton Instruments). As shown in Figs. 2(a), 2(b) and 2(c), the output beams exhibit a comb-like spectrum for both SOPOs, with spans exceeding 54 nm and 80 nm, or 14.3 THz and 21.2 THz, for the 140 μm and 485.25 μm SOPOs, respectively. The line spacings measure 514.0 GHz and 133.0 GHz, respectively, which are in good agreement with cavity lengths of 140 μm and 485.25 μm. Although the 140 μm SOPO has a larger CPM bandwidth in theory, its higher threshold prevents us from achieving a broader spectral span. This could potentially be improved by further increasing the Q in future studies.

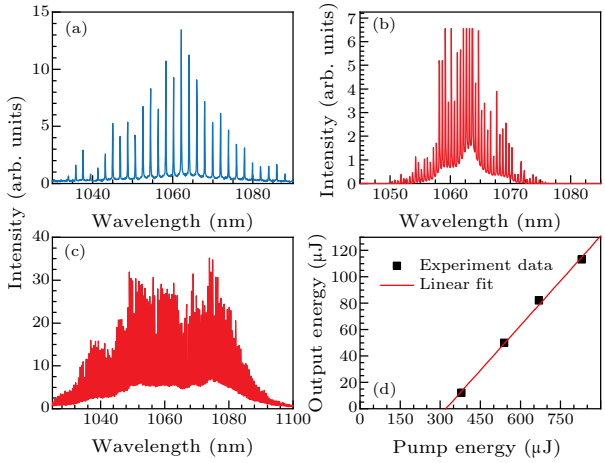

Fig. 2. SOPO spectrum and output pulse energy. Spectra of (a) 140 μm SOPO at 1.03 mJ pump. (b) 485.25 μm SOPO at 540 μJ pump, and (c) at 830 μJ pump. (d) Output pulse energy as a function of pump pulse energy. Output power of 130 μJ is measured, with a high slope efficiency of 22.6%.

The thresholds for parametric oscillation are 860 μJ and 320 μJ for the 140 μm and 485.25 μm cavities, with maximum output pulse energies of 42 μJ and 113 μJ at pump energies of 1.03 mJ and 830 μJ, respectively. We measure the output pulse energy as a function of that of the pump for the 485.25 μm SOPO. The result is shown in Fig. 2(d). The maximum conversion and slope efficiency are calculated to be 13.6% and 22.6%, respectively. Under the condition of maximum output, a peak power of 14.9 kW can be calculated, taking into account the measured 5.5 ns pulse width. Compared to the type-Ⅱ CPM SOPO in our previous work,[34] the maximum conversion and slope efficiency are calculated to be 18.6% and 21.2%, and the spectral width is 14.6 THz.

The uniformity of the comb line spacing is a key feature of an optical frequency comb, and our SOPO also exhibits this uniformity within the transform-limited linewidth of this pulse-pumped case, for both experimental and theoretical approaches. Figure 3(a) shows a schematic of the line-to-line measurement setup. The output parametric beam is collimated, and directed to a high-resolution double-pass grating filter, so that each single spectral line can be filtered out individually. This grating filter comprises a high-efficiency ruled grating and a silver mirror, which reflects the first-order diffraction beam back to the grating for the second diffraction. By tuning the mirror angle, we can couple any line into the fiber for measurement. The optical frequency of each line is measured by a high-performance wavelength meter (WS-7, High finesse) with an absolute accuracy of 40 MHz. For simplicity, only signal spectral lines with higher frequency than degeneracy are measured, and we number these starting from #0 at the degenerate point. Our SOPO has a normal dispersion of 275.4 fs^2/mm[36] at 1064 nm; however, the measured lines tend to be uniformly spaced, within the accuracy limit of the wavelength meter, as shown in Fig. 3(b). The deviations of these lines from the equal-spacing distribution measure 7.6 MHz in root-mean-square value. This is in agreement with the sub 10 MHz relative accuracy of the wavelength meter, and is much smaller than the linewidth of a single line, which is transform-limited to about 200 MHz in such a pulse-pumped case. This experimental result also shows good agreement with that given by our simulation. We perform the simulation for such an optical parametric effect in the SOPO; only the second-order nonlinear optical effects are included in this simulation. In both experiment and simulation, the line spacing can deviate by up to 1.049 GHz from the natural resonance of the SOPO cavity. More interestingly, some lines (#21–24th modes from the degeneracy) on the side of spectrum oscillate in the high-order transverse modes to follow the equal spacing, and remain within the cavity resonances. In such a case, we must couple them into a multi-mode fiber, and sacrifice the accuracy to 160 MHz. This line-pulling effect can only be interpreted as a result of line-to-line nonlinear interaction. Such a line-to-line interaction is well-known in the $\chi^{(3)}$ μOPOs, where two adjacent lines can seed into the next adjacent resonance modes via four-wave mixing. Here, this interaction may be interpreted as a result of cascaded $\chi^{(2)}$ processes,[21–27] which is confirmed by our simulation, with only second-order nonlinearity. As shown in Fig. 3(c), starting from line pair, $\#+/-i$ ($\omega_{\pm i} = \frac{\omega_p}{2} \pm i\Omega$, where Ω is the line spacing), and its closest adjacent line pair, $\#+/-(i+1)$, the cavity-enhanced sum frequency generation (SFG) process between ω_{-i} and ω_{i+1} can be cavity phase-matched to generate $\omega_p + \Omega$. Difference frequency generation (DFG) occurs between this SFG light and line $\#-(i+1)$, with an output frequency of $\omega_i + 2\Omega$ into the $\#(i+2)$ resonance. This DFG process can seed into the optical parametric amplification (OPA) process, with pump light to lock the $\#(i+2)$ line, and cascade over the whole comb span to lock the comb at one uniform spacing.

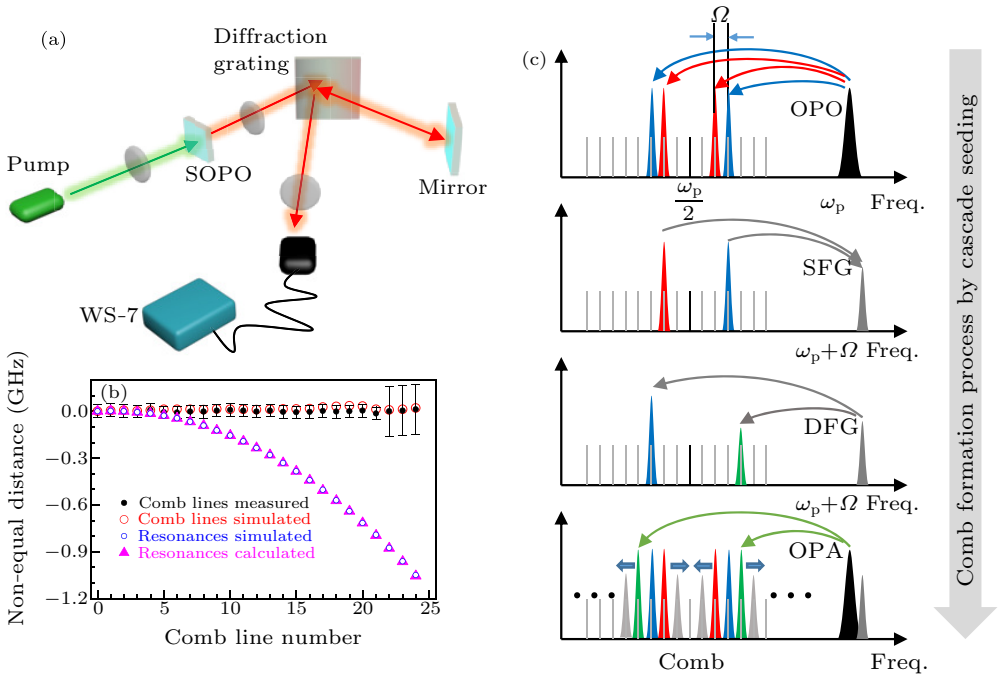

Fig. 3. Line-to-line measurement of the SOPO. (a) Experimental setup to measure the optical frequencies of individual spectral lines. (b) Spectral lines and μOPO resonance frequency deviations from equal spacing. Error bars show the instrument limit of wavelength meter. Lines #22–24 are in high-order transverse modes, and can only be detected via a multi-mode fiber, which results in reduced accuracy. (c) Schematic of the cascaded line-to-line interaction. The red, blue and green pairs denote the lines $\#+/-i$, $\#+/-(i+1)$, and $\#+/-(i+2)$. Starting from spectral line pairs $\#+/-i$ and $\#+/-(i+1)$, line pair $\#+/-(i+2)$ can be generated via cascaded SFG, DFG, and OPA processes. Such processes can be repeated for a coherent spectrum over the whole span.

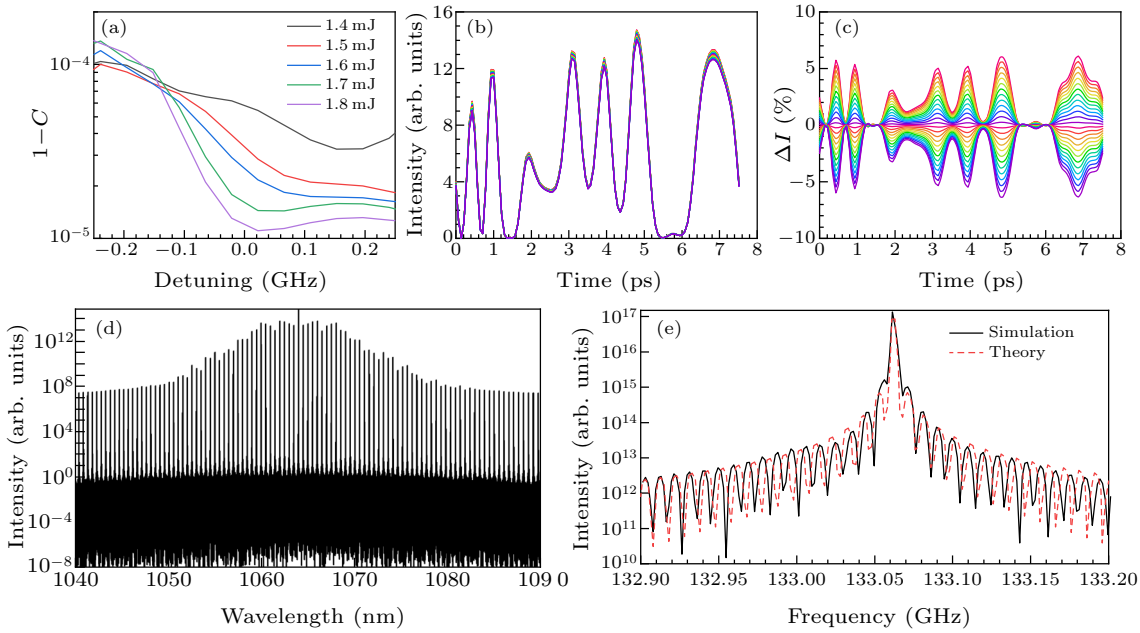

Fig. 4. Simulation of a 485.25 µm SOPO. (a) Noise level as a function of pump detuning at different pump powers (C: cross correlation). Here the comb noise can be characterized by the cross correlation between the temporal waveform inside one repetition and that of another repetition. A balance between noise and bandwidth can be achieved at 22 MHz pump detuning and 1.8 mJ pump, where the spectral and temporal behaviors are studied in detail. (b) Temporal profiles of 26 repetitions. (c) Relative intensity noise over 26 repetitions. The first repetition is used as reference and relative intensity noise is the difference between the intensity of the first repetition and others relative to the average intensity. (d) Spectrum of the SOPO. (e) Beat-note spectrum of the rf peak around the repetition frequency under a cw pump.

We perform a simulation using the split-step Fourier method, for the purpose of comparison with the experimental results. As shown in Fig. 4(a), we scan the pump, detuning υ at different pump levels to search for the lowest intensity noise, where $\upsilon = \omega_p - 2\Omega_0$, and Ω_0 is the central cavity resonance

frequency. The noise intensity shows similar behavior to the detuning changes at different pump power, and the lowest noise can be achieved when $\upsilon = 22$ MHz at 1.8 mJ pump. We plot 26 repetitions of the temporal waveforms under the above conditions; the results are shown in Fig. 4(b), and the relative noise plot in Fig. 4(c). The SOPO spectrum can be simulated via a Fourier transform of the temporal waveform, as shown in Fig. 4(d). It is interesting to compare the line spacings to the free spectrum range (FSR) of the cavity resonances in such a normal-depression SOPO cavity. Figure 4(e) shows the simulation result for the rf beat-note at a repetition frequency of around 133.06 GHz, and the linewidth is fit to be 1.67 MHz. Such linewidths and side band floors are limited by our simulation capability of 600 ns waveform length, as proven by a comparison with the theoretical beat-note spectrum in the red line, which can be achieved by choosing a stable repetition in time domain and reproducing a new periodic repetitive signal.

The pulse profile limits temporal uniformity, as well as the spectral resolution. With a cw pump, the temporal and spectral noise may be further reduced, as confirmed by our simulation. The spectrum noise is much lower than that for a pulse pump, and can be achieved when $\upsilon = -193$ MHz at 12 kW pump (for details, see the Supplementary Information). A high cw oscillation threshold of 10 kW for a bulk crystal SOPO makes the cw pump impractical. However, the cw-pumped SOPO is possible for higher-Q SOPO or waveguide devices. Our estimates show that a 100 W and 1 W threshold for cw comb generation can be achieved with a $Q = 6\times10^6$ SOPO and a $Q = 3.5\times10^5$ titanium diffusion waveguide,[38–40] respectively.

In summary, we have demonstrated a new approach to $\chi^{(2)}$ frequency comb generation in a sheet optical parametric oscillator via cavity phase-matching. Cavity phase-matching plays a key role in mitigating the stringent phase-matching condition imposed by a high-Q cavity, facilitating the achievement of a broader bandwidth of up to 21.2 THz. The slope efficiency and peak output power exceed 22.6% and 14.9 kW, respectively. SOPO lines are measured to be equally spaced within the accuracy of the wavelength meter, i.e., 40 MHz (or 160 MHz in for lines #21–24), suggesting the mechanism for an actual comb generation. The experimental results are supported and confirmed by our computer simulations, which also reveal the capacity of this approach to achieve a broad-band low-noise spectrum under cw pump. Therefore, this new $\chi^{(2)}$ SOPO platform represents a promising candidate for portable integrated optical frequency comb generation.

References

[1] Cundiff S T and Ye J 2003 *Rev. Mod. Phys.* **75** 325
[2] Udem T, Holzwarth R and Hänsch T W 2002 *Nature* **416** 233
[3] Coddington I, Swann W C, Nenadovic L *et al.* 2009 *Nat. Photon.* **3** 351
[4] Hillerkuss D, Schmogrow R, Schellinger T *et al.* 2011 *Nat. Photon.* **5** 364
[5] Pfeifle J, Brasch V, Lauermann M *et al.* 2014 *Nat. Photon.* **8** 375
[6] Li C H, Benedick A J, Fendel P *et al.* 2008 *Nature* **452** 610
[7] Wilken T, Curto G L, Probst R A *et al.* 2012 *Nature* **485** 611
[8] Diddams S A, Hollberg L and Mbele V 2007 *Nature* **445** 627
[9] Mandon J, Guelachvili G and Picque N 2009 *Nat. Photon.* **3** 99
[10] Ideguchi T, Holzner S, Bernhardt B *et al.* 2013 *Nature* **502** 355
[11] Marian A, Stowe M C, Lawall J R *et al.* 2004 *Science* **306** 2063
[12] Del'Haye P, Schliesser A, Arcizet O *et al.* 2007 *Nature* **450** 1214
[13] Kippenberg T J, Holzwarth R and Diddams S A 2011 *Science* **332** 555
[14] Huang S W, Yang J, Yu M *et al.* 2016 *Sci. Adv.* **2** e1501489
[15] Kim S, Han K, Wang C *et al.* 2017 *Nat. Commun.* **8** 372
[16] Dutt A, Joshi C, Ji X, Cardenas J, Okawachi Y, Luke K, Gaeta A L and Lipson M 2018 *Sci. Adv.* **4** e1701858
[17] Spencer D T, Lee S H, Oh D Y *et al.* 2018 *Nature* **557** 81
[18] Matsko A B, Savchenkov A A, Strekalov D *et al.* 2005 *Phys. Rev. A* **71** 033804
[19] Beckmann T, Linnenbank H, Steigerwald H, Sturman B, Haertle D, Buse K and Breunig I 2011 *Phys. Rev. Lett.* **106** 143903
[20] Fürst J U, Strekalov D V, Elser D *et al.* 2010 *Phys. Rev. Lett.* **105** 263904
[21] Ricciardi I, Mosca S, Parisi M *et al.* 2015 *Phys. Rev. A* **91** 063839
[22] Mosca S, Ricciardi I, Parisi M *et al.* 2016 *Nanophotonics* **5** 316
[23] Hansson T, Leo F, Erkintalo M *et al.* 2017 *Phys. Rev. A* **95** 013805
[24] Ikuta R, Asano M, Tani R *et al.* 2018 *Opt. Express* **26** 15551
[25] Xue X, Leo F, Xuan Y *et al.* 2017 *Light: Sci. Appl.* **6** e16253
[26] Ru Q, Loparo Z E, Zhang X *et al.* 2017 *Opt. Lett.* **42** 4756
[27] Mosca S, Parisi M, Ricciardi I *et al.* 2018 *Phys. Rev. Lett.* **121** 093903
[28] Armstrong J A, Bloembergen N, Ducuing J and Pershan P S 1962 *Phys. Rev.* **127** 1918
[29] Rosencher E, Vinter B and Berger V 1995 *J. Appl. Phys.* **78** 6042
[30] Berger V, Marcadet X and Nagle J 1998 *Pure Appl. Opt.* **7** 319
[31] Haïdar R, Forget N and Rosencher E 2003 *IEEE J. Quantum Electron.* **39** 569
[32] Clément Q, Melkonian J M, Raybaut M, Dherbecourt J B, Godard A, Boulanger B and Lefebvre M 2015 *J. Opt. Soc. Am. B* **32** 52
[33] Raybaut M, Dherbecourt J B, Melkonian J M, Godard A, Lefebvre M and Rosencher E 2013 *Proc. SPIE* **8631** 86311S
[34] Xie Z D, Lv X J, Liu Y H *et al.* 2011 *Phys. Rev. Lett.* **106** 083901
[35] Ciattoni A, Marini A, Rizza C and Conti C 2017 *Light: Sci. Appl.* **7** 5
[36] Zelmon D E, Small D L and Jundt D 1997 *J. Opt. Soc. Am. B* **14** 3319
[37] Ershova A L A G I, Kitaeva G K, Kulik S P, Naumova I I and Tarasenko V V 1991 *Sov. J. Quantum Electron.* **21** 225
[38] Pomarico E, Sanguinetti B, Gisin N, Thew R, Zbinden H, Schreiber G, Thomas A and Sohler W 2009 *New J. Phys.* **11** 113042
[39] Luo K H, Herrmann H, Krapick S, Brecht B, Ricken R, Quiring V, Suche H, Sohler W and Silberhorn C 2015 *New J. Phys.* **17** 073039
[40] Pomarico E, Sanguinetti B, Osorio C I, Herrmann H and Thew R T 2012 *New J. Phys.* **14** 033008

Supplementary Information for "Broadband Sheet Parametric Oscillator towards $\chi^{(2)}$ Optical Frequency Comb Generation via Cavity Phase Matching"

Xin Ni[1], Kunpeng Jia[1], Xiaohan Wang[1], Huaying Liu[1], Jian Guo[1], Shu-Wei Huang[2], Baicheng Yao[3], Nicolò Sernicola[1,4], Zhenlin Wang[1], Xinjie Lv[1*], Gang Zhao[1*], Zhenda Xie[1*] and Shi-Ning Zhu[1]

[1] *National Laboratory of Solid State Microstructures, School of Physics, College of Engineering and Applied Sciences, and School of Electronic Science and Engineering, Nanjing University, Nanjing 210093, China*

[2] *Department of Electrical, Computer, and Energy Engineering, University of Colorado Boulder, Boulder, CO 80301, United States*

[3] *Key Laboratory of Optical Fiber Sensing and Communications (Education Ministry of China), University of Electronic Science and Technology of China, Chengdu 611731, China*

[4] *Institute for optics, information and photonics, Friedrich Alexander university Erlangen-Nuremberg, Erlangen 91058, Germany*

[*] *Corresponding author. Email:* xiezhenda@nju.edu.cn(Z.D.X.), *Telephone:* +0086-18936027783(Z.D.X.);

Email: zhaogang@nju.edu.cn(G.Z.), *Telephone: 86-25-83593091* (G.Z.);

Email: lvxinjie@nju.edu.cn (X.J.L.), *Telephone:* +0086-15850515914 (X.J.L.);

I. Simulation of the frequency comb generation dynamics

In this simulation, we model the comb generation process in SOPOs with only second order nonlinearity. The light field evolution is simulated through split-step Fourier method [1], which is a pseudo-spectral numerical method to solve nonlinear

partial differential equations, such as the nonlinear Schrödinger equation in our case. An optical parametric oscillation (OPO) process can be treated as the combination of the nonlinear optical interaction and the linear propagation. In the split-step Fourier method, the OPO process is split into small alternating steps, with nonlinear interaction and linear propagation, respectively. While the nonlinear step is calculated in time domain, the linear step is calculated in the time domain, for maximum simulation efficiency, and Fourier transform is performed between steps for continuous simulation.

In an OPO process, a pump photon scatters into two photons with lower frequencies, which are called signal and idler. We can name the electric field of these three light waves E_p, E_s and E_i, respectively. While the E_p is transform limited in the spectral domain, the E_s and E_i spectrum is much broader due to the high cavity phase matching bandwidth. However, we can still define the carrier frequencies ω_p, ω_s and ω_i of all the three light fields, and the spectral broadening is attributed to the temporal modulation over these carrier waves. Here we can have a maximum bandwidth on the order of 10 *THz*, and thus temporal resolution better than 0.1 *ps* is required from the nature of Fourier transform.

For nonlinear transmission process, the split-step Fourier method is adopted to simplify the calculation steps:

$$E_s(z+\Delta h,t) \approx F_T^{-1}\exp\left(\Delta h\widehat{D}\right)F_T\exp\left(\Delta h\widehat{N}\right)E_s(z,t). \quad (1)$$

where Δh is the step length, $\widehat{D}$ is the linear operator representing linear propagation, and $\widehat{N}$ is the nonlinear operator representing nonlinear conversion process.

It is well known that the three-wave nonlinear coupling equations can be expressed as:

$$\begin{aligned}
\left(\frac{\partial}{\partial z}+\beta_p\frac{\partial}{\partial t}+i\frac{\gamma_p}{2}\frac{\partial^2}{\partial t^2}\right)E_p &= -\alpha_p E_p + i\frac{\omega_p d_{eff}}{n_p c}E_s E_i\exp(+i\Delta kz),\\
\left(\frac{\partial}{\partial z}+\beta_s\frac{\partial}{\partial t}+i\frac{\gamma_s}{2}\frac{\partial^2}{\partial t^2}\right)E_s &= -\alpha_s E_s + i\frac{\omega_s d_{eff}}{n_s c}E_p E_i^*\exp(-i\Delta kz), \quad (2)\\
\left(\frac{\partial}{\partial z}+\beta_i\frac{\partial}{\partial t}+i\frac{\gamma_i}{2}\frac{\partial^2}{\partial t^2}\right)E_i &= -\alpha_i E_i + i\frac{\omega_i d_{eff}}{n_i c}E_p E_s^*\exp(-i\Delta kz),
\end{aligned}$$

where the subscripts p, s and i represent for pump, signal and idler, respectively. β is related to the group velocity by $\upsilon = 1/\beta = c/n_g$, where the group index $n_g = n + \omega\frac{\delta n}{\delta\omega}$; and $\gamma = \frac{\delta}{\delta\omega}\left(\frac{1}{v_g}\right)$ is the group velocity dispersion. The frequency dependent refractive index n(ω) of the MgO doped Lithium Niobate n(ω) is derived from Sellmeier equation in Ref. [2], and Δk is the phase-velocity mismatch for the carrier frequencies, which is defined by

$$\Delta k = k_p - k_s - k_i, \tag{3}$$

and the carrier frequencies satisfy the energy conservation

$$\omega_p = \omega_s + \omega_i. \tag{4}$$

Taking the signal field as example, in the linear propagation step:

$$\left(\frac{\partial}{\partial z} + \beta_s\frac{\partial}{\partial t} + i\frac{\gamma_s}{2}\frac{\partial^2}{\partial t^2} + \alpha_s\right)E_s = 0, \tag{5}$$

a coordinate transformation is performed to a reference frame that moves with the speed v_m of the fastest wave among pump, signal and idler.

Performing a Fourier transformation of Eq. (5) into frequency domain, and substituting $\frac{\delta}{\delta t}$ with $i\omega$

$$\left(\frac{\partial}{\partial z} + i\omega\left(\frac{1}{v_s} - \frac{1}{v_m}\right) - i\omega^2\frac{\gamma_s}{2} + \alpha_s\right)E_s = \left(\frac{\partial}{\partial z} - \widehat{D}\right)E_s = 0, \tag{6}$$

where we define the linear transmission operator $\widehat{D}$ for the description of the propagation effect inside crystal.

Considering Eq. (2), the three-wave coupling is simulated in the nonlinear interaction step, which is solved using the nonlinear operator $\widehat{N}$:

$$\widehat{N}E_s = \frac{\partial}{\partial z}E_s = \frac{i\omega_s d_{eff}}{n_s c}E_p E_i^* \exp(i\Delta k z). \tag{7}$$

Thus the field evolution after every step period Δh can be written as

$$\frac{\partial E_s}{\partial z} = [\widehat{N} + \widehat{D}]E_s, \tag{8}$$

which can be solved as:

$$E_s(z + \Delta h, t) \approx F_T^{-1}\exp\left(\Delta h\widehat{D}\right)F_T\exp\left(\Delta h\widehat{N}\right)E_s(z, t). \tag{9}$$

The pump and idler fields can be derived in a similar way.

II. Simulation of the frequency comb generation in the pulse pump case

To simulated the pulsed pump case in our experiment, the pump light is treated as a pulse envelope, with central frequency of Ω_p, and we define the carrier frequencies of signal and idler Ω_s and Ω_i, respectively. The comb-line frequencies that deviate from Ω_s and Ω_i can be considered as results of time modulation over such carrier frequencies. In the Fourier transform of our split-step method, the step size Δh of the electric field evolution is chosen small enough to achieve the over 10THz broadening around Ω_s and Ω_i.

The SOPO consists two mirrors as linear resonator, where M1 is a total reflection mirror and M2 is an output coupler with a reflectivity of r. The nonlinear medium is filled between M1 and M2. The input signal and idler light fields are treated as vacuum quantum noise [5], and pump light field is treated as generalized Gaussian pulse of 10ns full width half maximum. The parametric light can recirculate in the 485.25 μm-thick SOPO for about 1400 times. After each circulattion, the backward intracavity field $\mathrm{E}_c^{'}$ can be related to the forward field by E_c with $\mathrm{E}_c^{'} = E_c \times r + E_{in} \times \mathrm{t}$, and the output filed E_{out} can be derived as $\mathrm{E}_{\mathrm{out}} = E_c \times t + E_{in} \times r$. Here t and r is M2's transmission and reflectivity, satisfying $\mathrm{r}^2 + t^2 = 1$. In our experiment, Q value of the SOPO is measured to be 1.9×10^5, which corresponds to an effective reflectivity of 93.23%, and it is used in the following simulation.

The relative relation between pump frequency and cavity resonance frequency is important for the comb generation. We choose the center of SOPO resonance frequency Ω_C to be close to $\Omega_p/2$, so that the energy conservation can be achieved. Moreover, it is important to slightly detune Ω_C in respective to $\Omega_p/2$ for a coherent comb generation. To achieve the optimal detuning, the influence of nonlinear dynamics on comb noise have been studied in simulation:

$$N_{comb} = 1 - C_{corr}(T) = 1 - \frac{\int r(t)s(t-T)dt}{\sqrt{\int |r(t)|^2 \, dt \int |s(t)|^2 \, dt}} \tag{10}$$

where temporal noise function N_{comb} can be characterized by the cross correlation $C_{\text{corr}}(T)$ between the temporal waveform inside one repetition r(t) and that of another repetition. In the ideal case of a coherent comb generation, the temporal waveform should repeat itself at the repletion time T, which is defined by the recirculating time of the SOPO cavity. By calculating the autocorrelation of the entire waveform, the repletion time T=7.51485ps can be obtained, which is shown in Fig. S1(a) and Fig. S1(b). The cross correlation approaches unitary in this case, and results in a low comb noise.

In the simulation, we scan the pump detuning υ at different pump levels to search for the lowest comb noise, where $\upsilon = \omega_p - 2\Omega_0$ and Ω_0 is the central cavity resonance frequency. We scan the pump energy from 1.4 to 1.8mJ and the lowest comb noise can be achieved when $\upsilon = 22MHz$ at 1.8mJ pump, which is shown in Fig 4a. Under the above conditions, a time frame of 26 repetitions are ploted together for a comparision, as shown in Fig. 4b. It is shown that these waveforms match each other very well. To visually see the residue noise over these repetitions, We define the relative intensity noise *RIN*:

$$RIN = (delta_I / \bar{I})_{(m,n)} = \frac{I_{(m,n)} - I_{(1,n)}}{\frac{1}{M}\frac{1}{N}\sum_{i=1}^{M}\sum_{j=1}^{N} I_{(i,j)}} \tag{11}$$

The first repetition is used as reference and we calculate the difference between the intensity of the first repetition and others relative to the average intensity. Here, m represents the serial number of repetitions and n indicates the serial number of the points in one repetition. To further characterize the noise level over the larger time scale, we study the RF beat-note of the whole pulse around the repetition frequency. The result in Fig. S1(f) shows a clean RF peak around 133.06GHz, and the linewidth is fit to be 140MHz, which is close to the Fourier transform limit of the pulse envelope.

The SOPO comb spectrum can be simulated by the Fourier transform of the temporal waveform, and it is shown in Fig. 4d. It is interesting to compare the comb

line spacings to the free spectrum range (FSR) of the cavity resonances in such a normal depression SOPO cavity. As shown in Fig. S1(d), we simulated the FSR by filtering a white light using the SOPO cavity (black dots), and the dispersion can cause an FSR change of over 300MHz within the comb span, and this result is in well-agreement with the calculated resonances using Sellmeier equation (red line). However, the comb lines can be pulled over 150MHz away to remain equally spaced (blue dots), and it agrees well with our experiment measurement as described in the main text (green dots).

III. Simulation of the frequency comb generation in the continues-wave pump case

In above simulation, the numerical results match well with our experimental measurement, and reveal the comb generation dynamics in the pulse pump case. As referred in the main text, the continuous pump can further improve the spectral accuracy and reduce the comb noise.

This simulation is still performed by the split-step method as described in Section I. We scan the pump detuning at different pump power for lowest comb noise. Due to the high accuracy of the CW pump case, we have to search for the repetition time by the autocorrelation calculation of the entire waveform in the time domain at each scan. Fig. S2(a) shows the result of such autocorrelation calculation with -193 *MHz* detuning at 12 *kW* pump, and Fig. S2(b) (c) the repletion time T=7.5153ps can be obtained with high accuracy. We plot 266 repetitions of the temporal waveforms under above condition and the result is shown in Fig. S2(d), and it can be found that these waveforms match each other very well. In fact, they are matched so well that we have to visually see them in the relative noise plot in Fig. S2(e), and the relative noise is less than 0.13%.The spectral behavior of the SOPO comb is also studied, and Fig. S2(f) is the simulated comb spectrum, with over 50nm span. We also simulated the comb spectral evolution in the 10^5 round trips, which shows how the comb evolves until stable, as shown in Fig. S2(g).

In conclusion, we have developed a split-step method to simulate the dynamics of the frequency comb generation in $\chi^{(2)}$ sheet-like μOPO. The simulation result shows that the comb generation with pristine line spacing can be achieved with only second-order nonlinearity, which supports our experimental results. Further investigation in the CW-pump case reveals that high quality comb is possible from such $\chi^{(2)}$ SOPOs, and it is a new approach for the micro-resonator comb study.

FIFURE

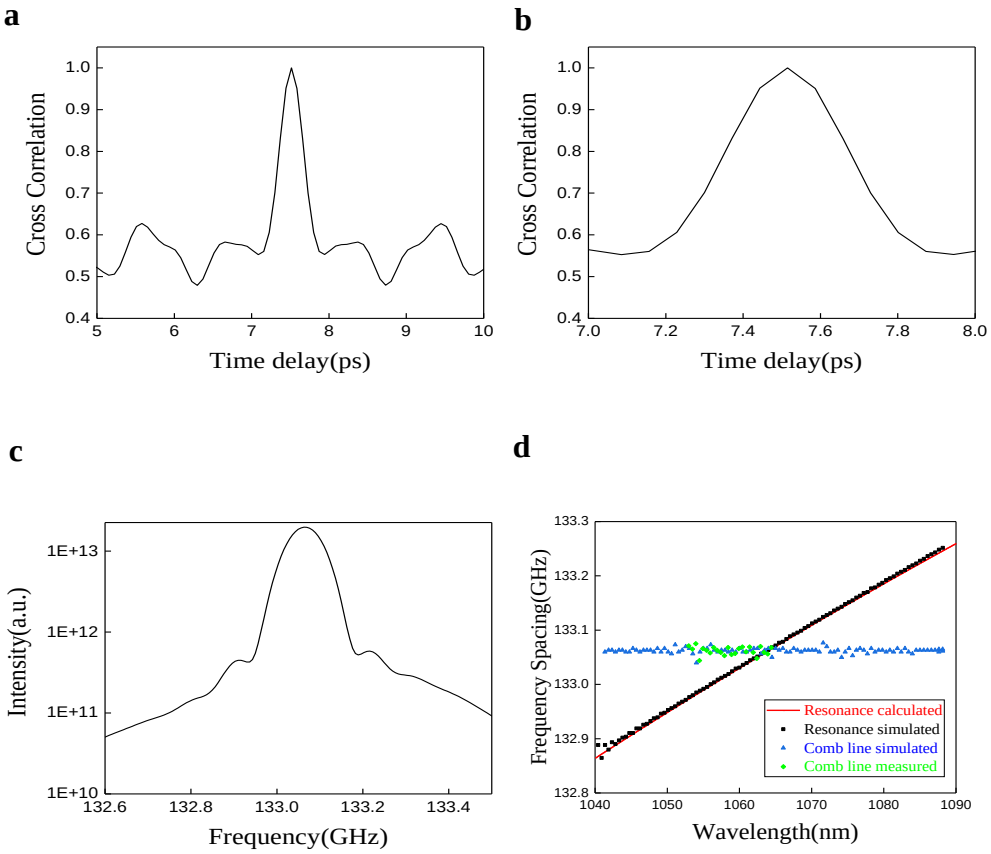

Supplementary Figure S1 | The simulation of the comb generation under pulse pump. **a.** Autocorrelation of the whole time domain waveform**. b.** Zoom in the autocorrelation of the whole time domain waveform and achieve the repetition period T=7.5153ps. **c.** The beat-note spectrum of the first RF peak. **d.** The comparison of the comb line spacing to the cavity resonances.

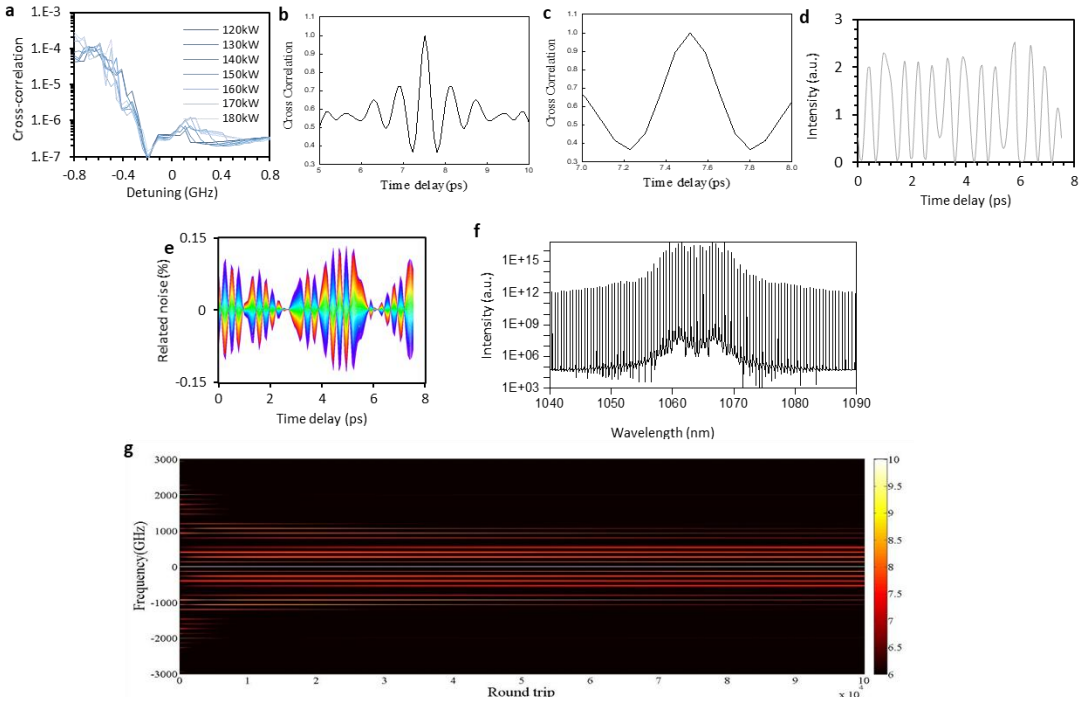

Supplementary Figure S2 | The simulation of the comb generation under CW pump. a. The noise level as a function of pump detuning at different pump power. The lowest noise can be achieved at -193 MHz pump detuning and 12 kW pump, where the spectral and temporal behaviors are studied in detail. **b.** Autocorrelation of the whole time domain waveform**. c.** Zoom in the autocorrelation of the whole time domain waveform and achieve the repetition period T=7.5153ps. **d.** The temporal profiles of 266 repetitions. **e.** The relative intensity noise of 266 repetitions. **f.** The output spectrum of continue wave pump. **g.** The corresponding spectral evolution map.

Supplementary References

[1] Smith A V, Gehr R J, Bowers M S. Numerical models of broad-bandwidth nanosecond optical parametric oscillators. J. Opt. Soc. Am. B 1998; 16**:**609-19

[2] Gayer O, Sacks Z, Galun E, et al., Erratum to: Temperature and wavelength dependent refractive index equations for MgO-doped congruent and stoichiometric $LiNbO_3$. Appl. Phys. B 2010; 101:481.